Journal of Materials Chemistry A

PAPER

View Article Online
View Journal | View Issue

Cite this: J. Mater. Chem. A, 2019, 7, 19495

Light-induced electrolyte improvement in cobalt tris(bipyridine)-mediated dye-sensitized solar cells†

Jiajia Gao,[a] Wenxing Yang,[b] Ahmed M. El-Zohry,[b] Govind Kumar Prajapati,[a] Yuan Fang,[a] Jing Dai,[a] Yan Hao,[a] Valentina Leandri,[a] Per H. Svensson,[ac] István Furó,[a] Gerrit Boschloo,[b] Torben Lund[d] and Lars Kloo *[a]

Received 4th July 2019
Accepted 1st August 2019

DOI: 10.1039/c9ta07198a

rsc.li/materials-a

Lithium-ion-free tris(2,2′-bipyridine) Co(II/III)-mediated electrolytes have previously been proposed for long-term stable dye-sensitized solar cells (DSSCs). Such redox systems also offer an impressive DSSC performance improvement under light soaking exposure, manifested by an increase in photocurrent and fill factor without the expense of decreasing photovoltage. Kinetic studies show that charge transfer and ion diffusion at the electrode/electrolyte interface are improved due to the light exposure. Control experiments reveal that the light effect is unambiguously associated with electrolyte components, $[Co(bpy)_3]^{3+}$ and the Lewis-base additive *tert*-butylpyridine (TBP). Electrochemical and spectroscopic investigation of the $[Co(bpy)_3]^{3+}$/TBP mixtures points out that the presence of TBP, which retards the electrolyte diffusion, however causes an irreversible redox reaction of $[Co(bpy)_3]^{3+}$ upon light exposure that improves the overall conductivity. This discovery not only provides a new strategy to mitigate the typical J_{sc}–V_{oc} trade-off in Co(II/III)-mediated DSSCs but also highlights the importance of investigating the photochemistry of a photoelectrochemical system.

Introduction

As a promising photovoltaic technology, dye-sensitized solar cells (DSSCs) have attracted much attention due to their expected advantages with respect to low-cost manufacturing and adaptive device structure based on the pioneering work of Grätzel and O'Regan in 1991.[1] Most efforts have been devoted to the engineering of the dye structure and the electrolyte formulation for broader spectral absorption and more efficient photon-to-electron conversion. It must be borne in mind that in a multi-component DSSC system, molecular configuration and composition could be changed because of dynamic equilibria through interactions between the components. Molecular dynamics and interactions at the dye/TiO_2 and TiO_2/electrolyte interfaces (mostly for traditional I^-/I_3^--based electrolytes) that closely correlate with interfacial charge transfer kinetics, have been well studied and illustrated in past decades. However, less attention has been dedicated to the one-electron, outer-sphere transition-metal complexes recently qualified as attractive redox shuttle alternatives. Such redox complexes in particular offer a high photovoltage of DSSCs,[4–7] and tunable redox potential and coordination sphere that can be used to control the driving forces and kinetics of the two rate-limiting electron transfer processes (including dye regeneration and electron recombination in the device[8,9]) *via* structural changes in the complex ligands.[7,10–12] Paradoxically, one-electron redox couples of this type offer fast regeneration of the oxidized dye molecules, but at the same time suffer from fast recombination loss reactions.[5,13–15] Co(II/III)-polypyridyl redox systems are the most studied and to date the most successfully employed in DSSCs, mainly due to the advantageous large inner-sphere reorganization energy necessarily for spin transition which reduces the interfacial charge-transfer loss.[9,16–18] Nevertheless, the recombination issue at the electrode/electrolyte interface still prevails for such redox mediators. One reason is attributed to the sluggish transport of the bulky complex ions, especially so when high-boiling and typically viscous solvents are used.[19] As a result, Co(III) ions attain a relatively high concentration at the interface that promotes recombination losses. In order to alleviate this issue, sensitizers with sterically bulky groups,[7,20] atomic layer deposition (ALD)[15,19] and potential-determining additives (PDAs), such as 4-*tert*-butylpyridine (TBP), are commonly employed to retard loss reactions at the TiO_2/dye/electrolyte interface. The retardation of recombination reaction rates is macroscopically observed as an improvement in the

[a]Division of Applied Physical Chemistry, Department of Chemistry, KTH Royal Institute of Technology, SE-100 44, Stockholm, Sweden. E-mail: larsa@kth.se
[b]Department of Chemistry, Ångström Laboratory, Uppsala University, Box 523, SE-75120, Uppsala, Sweden
[c]RISE Surface Process Formulation, Forskargatan 20j, SE-15136 Sodertalje, Sweden
[d]Department of Science and Environment, Roskilde University, DK-4000 Roskilde, Denmark

† Electronic supplementary information (ESI) available: Dye structures, photovoltaic performance of DSSCs, IPCE, Toolbox, electron injection and dye regeneration kinetic data, ^{1}H NMR and infrared absorption spectra. See DOI: 10.1039/c9ta07198a

open-circuit voltage.[2,21] The inclusion of polarizing ions at or close to the semiconductor surface, *e.g.* Li^+ or Mg^{2+} at the TiO_2 surface, also cause similar effects by changing the local distribution of cobalt cations and in particular, reducing the concentration of $[Co(bpy)_3]^{3+}$ (or Co(III) for simplicity) in the electric double layer at the photoanode surface.[18] Thus, the interaction between co-additives and the positively charged $[Co(bpy)_3]^{2+/3+}$ mediators, which by necessity must influence the function of $[Co(bpy)_3]^{2+/3+}$ in the device, calls for a more detailed study.

Related interactions could include the involvement of the additive TBP, which has been commonly used in DSSCs. TBP as a strong Lewis base is a likely competitive ligand for coordination to the cobalt centres based on evidence regarding the instability of cobalt tris(bipyridine) complexes through ligand exchange.[10,11,22,23] In addition, TBP was claimed by Salim *et al.* to exhibit a shielding effect with respect to the $[Co(bpy)_3]^{3+}$ ions *via* weak ion-dipole attraction accounting for the retarding role in the recombination loss reactions.[21] This work will further explore the interaction between the two necessary electrolyte components in a lithium-ion-free $[Co(bpy)_3]^{2+/3+}$-based DSSC system, where a high concentration of $[Co(bpy)_3]^{3+}$ is used since it has been demonstrated beneficial for long-term device stability.[2] In previous work, we have identified the role of TBP in promoting both the photovoltage and the photocurrent for this type of system. In this work, we will investigate the origin of a remarkable DSSC efficiency improvement after exposure to light.[2,3] The beneficial effects of light soaking, on the short-circuit current in particular, can be traced to a lowering of the conduction band edge of the semiconductor substrate, or alternatively to an increase in the density of states (or photo-induced surface states) facilitating the electron injection process.[24] Typically, such changes are considered to be caused by a photo-induced charge separation of the dye or semiconductor at open circuit changing the local electric field and thus causing a re-arrangement of charged species at the TiO_2/dye/electrolyte interface.[24–29] However, this work provides a new perspective, in which the electrolyte is involved in the light soaking effect. Control experiments based on the electrolyte components reveal that the light-induced change is associated with the combination of $[Co(bpy)_3]^{3+}$ and TBP. Changes in the electrochemical and spectroscopic properties have been studied and a new type of interaction between the two compounds is revealed.

Experimental section

Materials

All chemicals were purchased from Sigma Aldrich unless otherwise noted: fluorine-doped tin oxide (FTO; Pilkington, TEC 15 Ω cm^{-2} & TEC 7 Ω cm^{-2}), TiO_2 pastes (Dyesol Ltd., DSL 18NR-T and WER2-O), Surlyn frame (Solaronix). The dyes (D35, LEG4) and the tetracyanoborate or hexafluorophosphate salts of tris(2,2′-bipyridine-2*N*,*N*′) cobalt(II/III) were all obtained from Dyenamo AB, Sweden. All chemicals were of reagent grade and used without further purification.

Solar cell fabrication and characterization

The details of solar cell fabrication have been reported previously.[30] A transparent TiO_2 layer (diluted paste: a mixture of 60 wt% TiO_2 paste (DSL 18NR-T) with 36 wt% terpineol and 4 wt% ethyl cellulose; area: 0.5 cm × 0.5 cm, thickness: 5 μm) and a scattering layer (WER2-O, 3 μm) were in succession screen-printed on an FTO substrate (Pilkington, TEC 15 Ω cm^{-2}) with a TiO_2 blocking layer pre-deposited by a simple hydrothermal method. The working electrodes were sintered in the ambient atmosphere (325 °C for 25 min, thermostatic for 30 min, up to 500 °C for 25 min, thermostatic for 30 min and natural cooling), and post-treated with an aqueous $TiCl_4$ solution (40 mM). The working electrodes were dipped into a 0.25 mM D35/ethanol dye bath in the dark overnight. The platinized counter electrodes were prepared by drop-casting 20 μl of a 4.8 mM H_2PtCl_6 isopropanol solution on a pre-drilled and cleaned FTO (Pilkington, TEC 7 Ω cm^{-2}) glass substrate and then sintered in air at 400 °C for 30 min. The DSSC devices were fabricated by assembling the sensitized TiO_2 electrodes with the Pt counter electrodes into a sandwich-type cell using a 25 μm thick hot-melt Surlyn frame (inner area: 0.6 cm × 0.6 cm) as sealant, introducing the electrolyte through pre-drilled holes under atmospheric pressure, and sealing by a 50 μm thermoplastic sheet and a glass coverslip. A metal contact was soldered on the edge of the FTO film to increase conductivity. Measurements of the thickness of the TiO_2 layers were made by means of a profilometer (Veeco Dektak 150).

Current density–voltage (*J*–*V*) characteristics were recorded with a light-shading metal mask (0.7 cm × 0.7 cm) on top of the cell under standard irradiation (AM 1.5G, 100 mW cm^{-2}) supplied by a Newport solar simulator (model 91160-1000). Light illumination for incident photon-to-current conversion efficiency (IPCE) measurements was provided by a computer-controlled set-up assembled with a xenon arc lamp (300 W Cermax, ILC Technology), a monochromator (CVI Digikrom CM 110) and appropriate filters. Both *J*–*V* curves and IPCE spectra were recorded by a computerized Keithley 2400 source meter calibrated using a certified reference solar cell (Fraunhofer ISE).

Light exposure treatments performed on open-circuit solar cells and electrolyte samples were performed under continuous irradiation (~100 mW cm^{-2}, 390 nm UV cut-off; ATLAS Suntest XLS) in a sample compartment maintaining a temperature of 60 °C. Samples aged in the dark were subjected to the same temperature conditions (60 °C). Two different approaches were used in this study, as schematically visualized in Scheme 1, where either model electrolytes with only selected components were pre-exposed to light (the pre strategy) and subsequently complemented with the remaining components to complete the electrolyte, according to the composition given below, and then introduced into a DSSC to be further characterized. Alternatively, the DSSC was made in the standard way, then exposed to light (the post strategy) and characterized. The post strategy is the typical way to perform ageing tests of DSSCs. In this work, the main insights have been obtained through the pre strategy.

The electron lifetime (τ_n) and diffusion time (τ_d) in TiO_2 films were estimated by first-order models of the transient

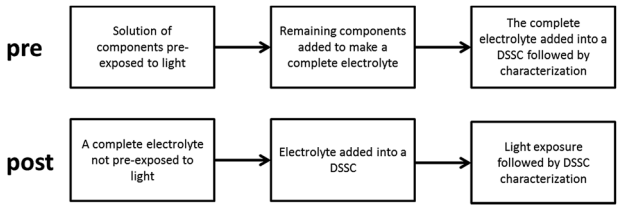

Scheme 1 A visualization of the two main strategies, pre and post, used in this work.

voltage and current decay traces, respectively, following a small square-wave modulation to the base light intensity varied by controlling a white LED (Luxeon Star 1 W). The decay traces were recorded using a 16 bit resolution digital acquisition board (National Instruments) in combination with a current preamplifier (Stanford Research Systems SR570) and a custom-made system with electromagnetic switches. The methods of measurement have been reported previously.[7,31] The relationship between voltage and extracted charge (Q_{oc}) under open-circuit conditions was studied using a combined voltage decay/charge-extraction method.[32] Relative data used in the figures were based on the best-performing cells for each type of electrolyte. Electrochemical impedance spectroscopy (EIS) measurements were conducted with an Autolab PGstat12 potentiostat with an impedance module. The frequency was swept from 10^5 Hz to 0.1 Hz using a 20 mV AC modulation amplitude. Electrochemical impedance spectra were recorded under dark conditions with an applied bias voltage. The curves were modeled using the Z-View software and an equivalent circuit model as shown in Scheme S1.†

Transient absorption measurements

Devices for transient absorption measurements were fabricated in the same way as the solar cells above, except that the photoanode contained a transparent TiO_2 layer (no scattering layer was applied). Nanosecond transient absorption measurements were performed using an Edinburgh Instrument LP920 laser flash photolysis spectrometer with continuous wave xenon light as the probe light and a photomultiplier tube detector (system response time, ~1 μs). Scattered light from the excitation was excluded with a 715 nm cut-on filter in front of the detector. Laser pulses were supplied by a Continuum Surelite II, Nd:YAG laser at a 10 Hz repetition rate in combination with an OPO (Continuum Surelite). The pulse intensity was attenuated to 0.2–3 mJ per pulse with the use of natural density filters. The pump light wavelength was selected to 530 nm. Kinetic traces of absorbance were detected at 760 nm, averaged over 50 to 100 pulses per sample. Three samples were prepared for each electrolyte composition, and the measurement error was estimated from the average deviation. The overlaid curves were modelled with a KWW function only for visualization. The kinetics of the system were characterized by the half time, $t_{1/2}$, of the decay of the initial absorption difference.[33] For the femtosecond transient absorption in the infrared region (IR), femtosecond laser pulses of 800 nm with a repetition rate of 3 kHz were used to generate an excitation wavelength of 520 nm with a power of 110–170 μW, and a probe pulse with a centered wavelength of *ca.* 5000 nm (~2000 cm^{-1}). More details about the femtosecond experimental setup can be found in previously published work.[34]

Electrochemical measurements in a symmetrical dummy cell

Symmetrical dummy cells were fabricated by assembling two identical platinized FTO glass plates with the incomplete model electrolytes in between containing only 0.15 M $[Co(bpy)_3]^{3+}$ and TBP in various concentrations with exposure to light for different time periods. All electrochemical measurements were carried out under dark conditions. The same set-up and conditions as described above were used for the EIS measurements. Resistance and capacitances were analysed using an equivalent circuit model, and the diffusion time (τ_d) was calculated according to literature methods.[35] Cyclic voltammograms (CVs) were recorded stepwise by increasing the scan rate from 10 to 250 mV s^{-1} with an interval waiting time of 100 s.

In situ characterization of $[Co(bpy)_3]^{3+}$/TBP mixtures

UV-vis absorption spectra were recorded on a Cary 300 spectrophotometer in a quartz sample cell (1 cm path length). Cyclic voltammetry and differential pulse voltammetry (DPV) measurements were conducted using an Autolab potentiostat with a glassy carbon disk as the working electrode, a platinum wire as the counter electrode and $Ag/AgNO_3$ as the reference electrode. 0.1 M $[Bu_4N]PF_6$ was added as conductive medium. The rest potential of the electrolyte was recorded by measuring the potential difference between the assembled electrode, composed of a Pt wire in contact with the target electrolyte in a plastic tube with a frit top allowing the free movement of ions, and an Ag/AgCl (1 M LiCl in ethanol) reference electrode in the supporting electrolytes (0.1 M $[TBA]PF_6$ in acetonitrile) with the use of a $6\frac{1}{2}$ digit precision digital Keithley 2700 source meter. The reference electrode potential was calibrated by Fc/Fc^+ in the same supporting electrolyte. The accuracy of the potentials determined was estimated to be around 5 mV.

The NMR-spectroscopic experiments were performed on a Bruker Advance III 500 MHz spectrometer equipped with a 5 mm high-resolution probe, which can provide a maximum of 0.5 T m^{-1} gradient in the z-direction. In the diffusion experiments a stimulated echo pulse sequence was used with gradient pulse length of $\delta = 3.0$ ms, a diffusion time $\Delta = 50$ ms and allowing the gradient to increase linearly from 0.02 to 0.22–0.35 T m^{-1} in 16 steps. Each spectrum was obtained from 16 scans. The gradient strength g was calibrated with a sample of deuterated water at 298 K. For eNMR measurements, a double stimulated echo pulse sequence with a bipolar voltage pulse was used with gradient pulse length $\delta = 1.0$ ms, drift time Δ_E of 100 ms and gradient strength of 0.32 T m^{-1}. The electric field E was incremented from 0 to 21 V cm^{-1} in at least 8 steps. All experiments were conducted at 293 K. The diffusion coefficients were obtained by modeling the signal attenuation with a conventional Stejskal–Tanner expression. The electrophoretic mobility

was obtained from the phase modulation by the electric field strength according to

$$\phi = \gamma g \delta \Delta_E \mu E$$

where μ is the electrophoretic mobility, γ is the gyromagnetic ratio and ϕ is the phase of target molecule. The phase was corrected as previously described[36] by using an uncharged molecule as reference to compensate for bulk flow from electro-osmosis and thermal convection. In this particular case the reference used was acetonitrile.

Computational details

Calculations were performed on $[Co(bpy)_3]^{3+}$ and various coordination species with partly or fully exchanged bpy ligands for TBP, with and without acetonitrile modelled as solvent. All calculations were performed using the Gaussian 09 program package,[37] including a selection of different functionals and hybrid functionals. All results presented are based on results from B3LYP including the Coulomb-attenuating method improving long-range exchange interaction.[38] A 10-electron effective-core pseudopotential (MDF10) was employed for Co including a (8s7p6d2f)/[6s5p3s2f] contracted valence space and basis sets of 6-311G type for all lighter elements.[39,40] The effects of the acetonitrile solvent were implicitly introduced using the Polarizable Continuum Model (PCM) as implemented in Gaussian 09.

Results and discussion

Light-induced efficiency enhancement

In this work, typical triphenylamine (TPA) based sensitizers with bulky chains (D35 and LEG4, see Fig. S1†) were employed, and cobalt-based electrolytes were prepared according to the same Li^+-free recipe as previously reported: 0.30 M/0.15 M $[Co(bpy)_3]^{2+/3+}$ and 0.2 M TBP in acetonitrile.[2] A higher than normal concentration of the Co(III) redox-system component (0.05 M) was used in this study to ensure efficient device performance in the absence of Li^+. Fig. 1 shows the chemical structures of $[Co(bpy)_3]^{2+/3+}$ and TBP, where the $Co^{2+/3+}$ centre adopts a quasi-octahedral coordination by N-atoms of the three bpy ligands. The acetonitrile solutions of systematically varied combinations of the three components: Co(II)/Co(III)/TBP, Co(II)/TBP, Co(III)/TBP, Co(III) only and TBP only were pre-exposed to light-soaking conditions (1 sun, 390 nm cut-off, 60 °C; denoted as the pre strategy in Scheme 1) before preparing the complete electrolyte and assembling the device; related DSSC efficiency (η) and short-circuit current (J_{sc}) were compared to non-light-treated complete electrolytes without and with assembled devices exposed to the same light treatment (denoted as the post strategy). By comparison, results in Fig. S2† show that the light-induced DSSC improvement in the post strategy can be achieved by the pre strategy based on the cobalt-based electrolyte and more specifically on the mixture of $[Co(bpy)_3]^{3+}$ and TBP only. This means that the beneficial light effect actually can be attributed to this mixture. For clarity, Fig. 2 and Table 1 show the performance of DSSCs assembled with different complete electrolytes: electrolyte A, non-treated; electrolyte A* and electrolyte A^T: according to the pre strategy part of the electrolyte containing $[Co(bpy)_3]^{3+}$/TBP/acetonitrile exposed to one sun irradiation (390 nm cut-off)/60 °C and stored in the dark/60 °C, respectively. The electrolyte A-Li^+ is the non-treated electrolyte A with additional 0.1 M $LiClO_4$ included for comparison.

The results clearly demonstrate that the effect of light exposure, rather than that of thermal stress, on the electrolyte causes a notable increase in photocurrent (by ~20%) and total efficiency (by ~25%) of the resulting devices. Both parameters and fill factor (FF) are comparable to those of devices containing added Li^+ salt, and notably the open-circuit voltage (V_{oc}) is quite high mitigating the typical J_{sc}–V_{oc} trade-off suffered by the addition of PDAs. The same results were obtained for devices based on other TPA-type dyes (LEG4), or cobalt redox couples with different counter ions (PF_6^-), see Table S1.† We also observed that the beneficial light effect is irreversible and remains stable after the illumination has been terminated. Consistently, the incident photon-to-current conversion efficiency (IPCE) within the spectral range investigated also increases and broadens towards the red, as shown in Fig. 2b and S3.† IPCE represents an integrated result of crucial processes occurring in DSSCs and is often expressed as

$$\mathrm{IPCE}(\lambda) = \varnothing_A(\lambda) \times \varnothing_{inj} \times \varnothing_{reg} \times \eta_{cc} \quad (1)$$

where $\varnothing_A(\lambda)$, $\varnothing_{inj}$, $\varnothing_{reg}$ and η_{cc}, represent the efficiency of light-harvesting, electron injection, dye regeneration and charge collection at a particular wavelength (λ), respectively. As shown in Fig. 2b, the absorption spectrum of the dye on a TiO_2 film shows no shift but is slightly extended to lower energies after the contact Co(III)/TBP solution has been exposed to light, therefore contributing to an increase in $\varnothing_A$ and thus the IPCE at longer wavelengths, mainly between 450 nm and 550 nm. The UV-vis band extension to the red region is less pronounced than observed for the corresponding IPCE spectra, indicating that the energy levels of TiO_2 could be shifted as well. The effect on the dye is different with respect to that of lithium salts, since the latter shows a total red-shift in the maximum absorption which has been attributed to a stabilisation of the sensitizer LUMO by the added Li^+ ions or to a Stark effect.[41–43] The spectral change indicates that a change in the electrolyte property (for instance, an increase in the solution acidity) occurs during light exposure and that the dye/TiO_2 interface is affected.[41,44] A coherent study was conducted on the electron transfer kinetics at the dye/TiO_2

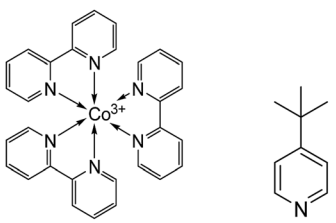

Fig. 1 Molecular structures of the tris(2,2′-bipyridine) cobalt(III) complex (left) and TBP (right).

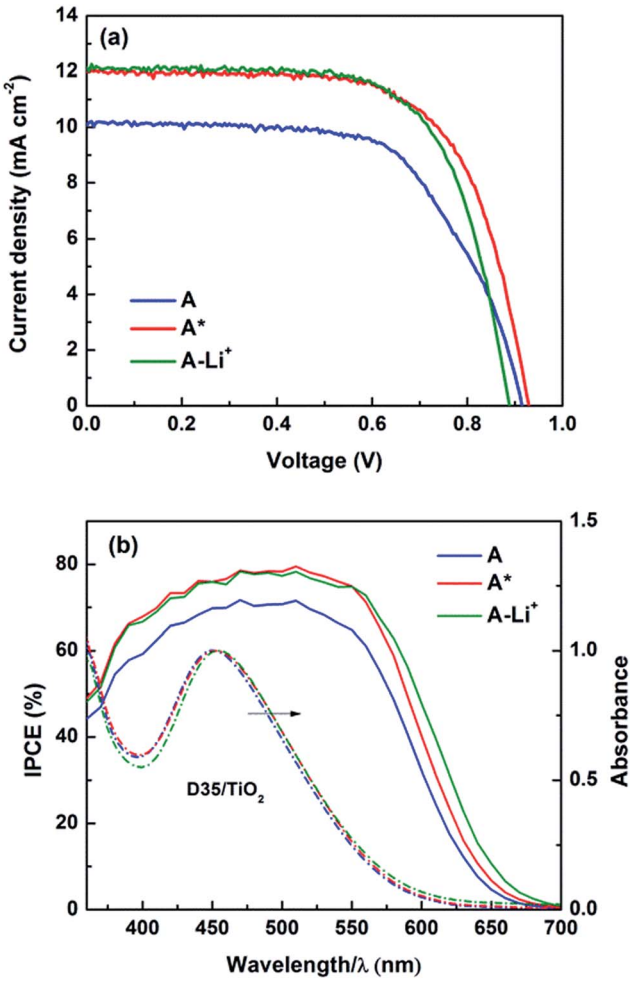

Fig. 2 (a) The J–V characteristics and (b) incident photon-to-current conversion efficiency (IPCE) spectra (solid lines) of D35-sensitized DSSCs assembled with $[Co(bpy)_3]^{2+/3+}$-based electrolytes, untreated (A, blue; A-Li$^+$, green) and treated by light as described in the main text (A*, red). In (b), normalized UV-vis absorption spectra (dashed lines) were recorded for D35 adsorbed onto the TiO_2 film in contact with the Co(III)/TBP acetonitrile solution before (blue) and after (red) light exposure, and with Li$^+$ salts added without light exposure (green). The absorption contribution of the contacting electrolyte was deducted.

interface using femtosecond IR studies on nanocrystalline TiO_2 thin films. As seen from Fig. S4 and Table S2,† the electron injection/recombination rates at the dye/TiO_2 surface are reduced when the contact Co(III)/TBP solution has been light-exposed. The difference, although less pronounced, demonstrates that the dye/TiO_2 coupling must be influenced by a certain component in the light-exposed solution. Based on the well-studied effects of the electrolyte composition on the interface,[44–46] we therefore propose that the light induces a change in the composition of the Co(III)/TBP solution.

Changes with respect to interfaces and kinetics in full devices

In order to elucidate the origin for the light-induced increase in IPCE and photocurrent, an investigation of the dye regeneration kinetics was performed; see the results in Fig. S5 and Table S3.†

Table 1 J–V characteristics for D35-sensitized solar cells based on electrolytes untreated (A, A-Li$^+$), and treated according to the pre strategy as described in the main text (A*, A^T)

Electrolytes[a]	V_{oc}/mV	J_{sc}/mA cm^{-2}	FF	η/%
A	900 ± 15	9.9 ± 0.2	0.63 ± 0.01	5.6 ± 0.3
A*	920 ± 10	11.9 ± 0.1	0.66 ± 0.01	7.2 ± 0.3
A^T	871 ± 14	9.6 ± 0.2	0.65 ± 0.01	5.4 ± 0.4
A-Li$^+$	877 ± 13	12.0 ± 0.2	0.67 ± 0.01	7.1 ± 0.2

[a] A* and A^T were composed of a pre-exposed $[Co(bpy)_3]^{3+}$/TBP mixture, light/60 °C and dark/60 °C conditions for 4 hours, respectively. Each data in the table present the average of three independent cells.

However, the difference in the half-time ($\tau_{1/2}$) of dye regeneration by the cobalt electrolyte is in the order of sub-microseconds. Previous studies on the D35 dye under similar conditions have revealed that the intrinsic charge recombination is in the order ~10 to 100 μs.[7] Thus, this small difference in the $\tau_{1/2}$ observed here would contribute negligibly to the dye regeneration efficiency, $\emptyset_{reg}$, and therefore cannot explain the large change in the IPCE nor in the J_{sc} observed in Fig. 2. Logically, it is instead expected that the photocurrent increase can be assigned to an increase in the product $\emptyset_{inj}\eta_{cc}$. Fig. 3a and S6a† show the evolution of DSSC performance as a function of time of light-exposure treatment (the pre strategy). It is clear that the J_{sc} and FF increase dramatically to a steady-state situation reached after 4 hours of exposure, while the V_{oc} stabilizes already after a slight increase in a considerably shorter time. In parallel, we monitored the change in the electron accumulation in the TiO_2 film and the interfacial transfer kinetics. As shown in Fig. S6b,† by prolonging the Co(III)/TBP-solution light pre-exposure, the charge storage in the dye/TiO_2 electrode at the same open-circuit voltage (or energy level) increases gradually, and the tail of the band-gap trap states is broadened. By exponential modelling of the distribution of trap states according to eqn (S1)–(S3),† it is notable that the difference in the TiO_2 conduction band energy level (E_c) and the electrolyte redox potential (E_{redox}) decreases by pre-exposure of the electrolyte to light, indicating that E_c is positively shifted (~0.1 eV) while E_{redox} remains almost constant; see Fig. S7 and Table S4.† As E_c is lowered, the density of electron-acceptor states in the TiO_2 film iso-energetic with the dye excited states also increases, and it is expected that the band edge downshift promotes a higher $\emptyset_{inj}$, especially at longer wavelengths.[24,28] From the electrolyte point of view, the origin of the E_c shift could be caused by electrolyte charging the TiO_2 surface; the E_c downshift is either caused by an increase in the surface positive charge (*e.g.* protons) or through a decrease in the negative charge; the latter is linked to TBP concentrations in the systems studied. However, we have previously demonstrated that a mere reduction in initial concentration of TBP in the cobalt electrolyte shows little improvement.[2] According to the results shown in Table S1 and Fig. S8,† by adding extra Lewis base (TBP or bipyridine) to the pre-exposed electrolytes, the downshift of the E_c is reduced and the improvement of the DSSC performance is also decreased. This means that the E_c shift constitutes a reason

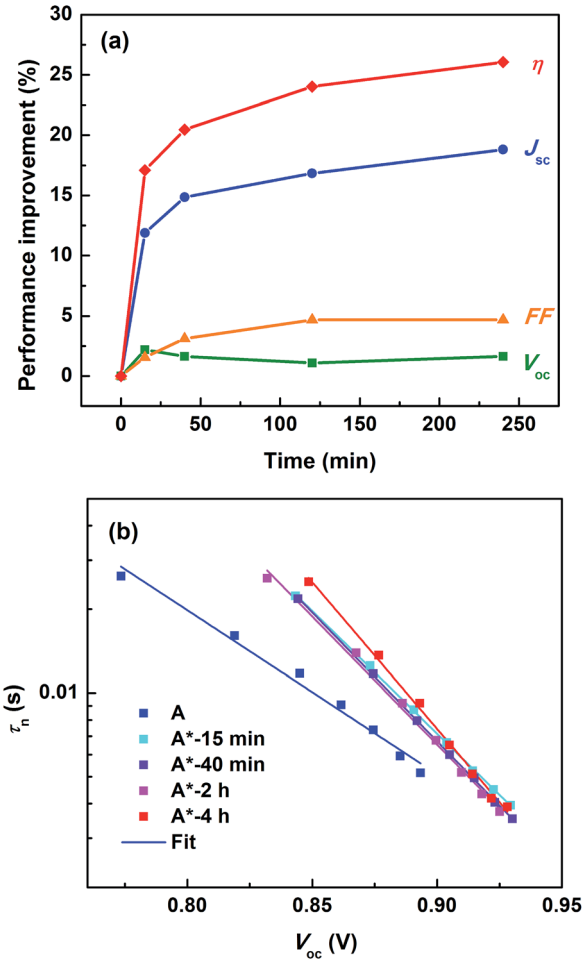

Fig. 3 (a) The photovoltaic performance improvement of DSSCs and (b) electron lifetime in D35-sensitized TiO_2 films as a function of light exposure time of the $[Co(bpy)_3]^{3+}$/TBP component in the electrolyte.

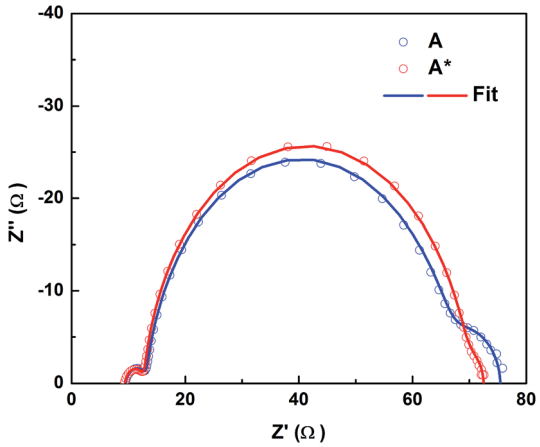

Fig. 4 Nyquist plots of D35-sensitized solar cells containing Co(III)/TBP electrolytes without (A) and with (A*) pre-exposure to light. The results were obtained from EIS measurements under dark conditions and at −0.9 V bias. Three semicircles in the plots represent: from left to right, the charge transfer resistances at the electrolyte/counter electrode interface, the charge-transfer resistance at the photoanode/electrolyte interface and the diffusion resistance of the electrolyte, respectively. Parameters obtained from the models are shown in Table S6.†

for the performance improvement, likely due to positive charges at the TiO_2/electrolyte interface produced in the $[Co(bpy)_3]^{3+}$/TBP electrolyte during light exposure.

The electron collection efficiency (η_{cc}) is determined by two competing processes, the electron diffusion time (τ_d) and the electron recombination time, *i.e.* electron lifetime (τ_n) in TiO_2, according to the relation of $\eta_{cc} = 1/(1 + \tau_d/\tau_n)$. It was noted that τ_n is increased when pre-exposed electrolytes are used, while the change in τ_d is negligible, see Fig. 3b and S6c.† This indicates that η_{cc} increases after the electrolyte is pre-exposed to light, which is consistent with the increase in the IPCE and photocurrent. τ_n directly reflects the interfacial recombination kinetics of the injected electrons from TiO_2 to the electrolyte; consistently, we observed a larger recombination resistance (the middle semicircle) in the light-exposed system in EIS results, see Fig. 4. In this perspective, two crucial factors need to be investigated: (1) Co(III) complexes, the concentration of which significantly influences the recombination loss rates operating as electron acceptors, and (2) interfacial recombination-suppressing additives, such as TBP or small cations; for the latter, Li^+ has been demonstrated to effectively improve τ_n in our previous work,[3] and in this work it could be protons being active in the Li^+-free electrolyte. A loss of Co(III) likely due to light-induced degradation could be a reason for the increase in τ_n; however, by comparing the performance of DSSCs differing in the concentration of initially added Co(III) without light exposure treatment (Table S5 and Fig. S9†), the effect on increasing τ_n is significantly less even when the concentration is lowered to half, and little improvement occurs in cell performance. Moving to the other potential factor, the way for TBP to retard electron recombination is proposed to be either by passivating the TiO_2 by surface adsorption, which promotes an increase in E_c as well, or by an impeding effect on the $[Co(bpy)_3]^{3+}$ complex, possibly in the form of 'shielding'.[21] The observed E_c downshift, as mentioned above, excludes the former TBP effect and also suggests adsorption of small cations, *e.g.* protons, probably as the reason. More noteworthy in Fig. 4 and Table S6† is that the pre-exposure treatment also causes a significant decrease in the diffusion resistance of the electrolyte from 10 Ω to 3 Ω, which may explain the increase in the current. In summary, the light-exposure strategy intrinsically solves the current-limiting issues of the classic cobalt-based electrolytes and irreversibly improves the performance of this type of DSSCs. Kinetics studies show a TiO_2 E_c downshift, retarded recombination and improved electrolyte diffusion, accounting for the significant increase in the photocurrent. The effects are directly tied to the combination of $[Co(bpy)_3]^{3+}$ and TBP, and an irreversible change induced by light exposure. Therefore, in the following section we focus on a more simple mixture, $[Co(bpy)_3]^{3+}$/TBP, to understand the chemistry involved.

Electrochemical studies on $[Co(bpy)_3]^{3+}$/TBP mixtures

The changes in the electrochemical properties of the $[Co(bpy)_3]^{3+}$/TBP acetonitrile solution before and after light exposure were investigated. Electrochemical studies of the

mixtures were conducted in a symmetrical dummy cell with platinized FTO glass electrodes. In Fig. 5, cyclic voltammetry (CV) results show that when TBP present, the current response is lower compared to solutions containing Co(III) alone (Fig. S10a†), and the peak current (i_p) shows a clear dependence on the scan rate (ν). The linearity in i_p as function of the square root of scan rate ($\nu^{1/2}$) (Fig. S11†) indicates that the charge transfer is controlled by ion diffusion. As shown in Fig. S12,† by comparing EIS results of the solution containing $[Co(bpy)_3]^{3+}$ alone with those also containing different concentrations of TBP, it is clear that introduction of TBP to the $[Co(bpy)_3]^{3+}$ electrolyte causes an increase in both diffusion resistance (R_d) and diffusion time (τ_d). In principle, $\tau_d = L^2/D$, where L is the electrolyte layer thickness and D is the effective diffusion coefficient of the limiting species. Thus, the diffusion limit originates from the retarding effect of TBP and probably a lower diffusion coefficient of the limiting species. Previous work has attributed this effect to the high viscosity of TBP.[47] This effect has also been noted by Kirner and Elliot suggesting a Co(III) ligand exchange involving TBP.[48] Based on our previous work,[2] the adsorption of TBP molecules could influence the surface property of the Pt electrode and thus the charge transport kinetics. After light exposure, CVs of the TBP-containing system show no scan-rate dependence and a 3-fold limiting current. This indicates that the charge transfer process turns to redox kinetic control, and the mass transport in the system is greatly improved. We added the reduced cobalt component ($[Co(bpy)_3]^{2+}$, 0.3 M) to the exposed system to complete the electrolyte. A higher I–V slope was observed but almost the same limiting current, see Fig. S10b.† Such a comparison demonstrates that increasing the concentration of Co(II) (the rate-limiting species) improves the redox kinetics and reversibility in the symmetric cell system, but it does not influence the diffusion. Consistently, τ_d decreases to 1/3, indicating that the diffusion kinetics at the electrode/electrolyte interface is improved, either through an increase in the diffusion coefficient of the limiting species or a change in the electrode surface environment. These results explain the decrease in the diffusion resistance to one third for a complete cell after pre-exposure treatment as depicted in previous section.

In summary, the higher charge-transport ability of light-exposed electrolytes in the presence of $[Co(bpy)_3]^{3+}$ and TBP is notable, and the link to the better photovoltaic properties is clear. However, the reasons at a molecular level are less obvious.

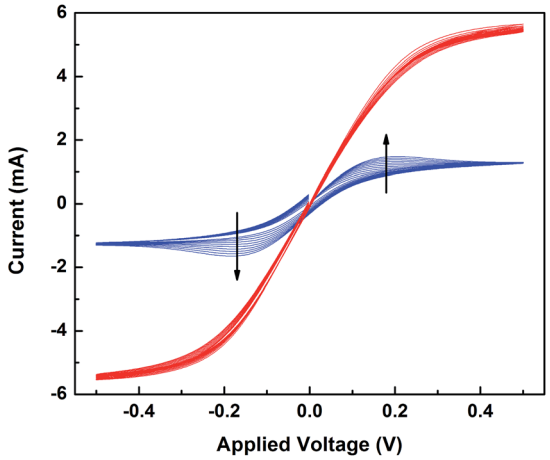

Fig. 5 Cyclic voltammograms of 0.15 M/0.2 M $[Co(bpy)_3]^{3+}$/TBP electrolytes in acetonitrile; fresh (blue) and after light exposure (red), symmetrical dummy cells at scan rates from 25 mV s^{-1} to 250 mV s^{-1}, interspace 25 mV s^{-1}. The arrows show the direction of change with increasing scan rate.

Spectroscopic studies on $[Co(bpy)_3]^{3+}$/TBP mixtures

In order to identify the origin of the light effect at a molecular level, we investigated the $[Co(bpy)_3]^{3+}$/TBP mixture using different spectroscopic techniques. From a coordination chemistry perspective, the $[Co(bpy)_3]^{3+}$ complex can be regarded as a quasi-octahedral d^6 system, and using a simple ligand-field-inspired model it is expected that the $[Co(bpy)_3]^{3+}$ complex is diamagnetic (low spin) and that d–d absorption bands are weak, consistent with the UV-vis absorption features in Fig. 6, because the 6 (mainly) d-type electrons are located in a (near)degenerate orbital of t_{2g} symmetry. Upon mixing with TBP and before light exposure, the absorption spectrum of $[Co(bpy)_3]^{3+}$ in the visible region shows a notable change: a new absorption band at ~425 nm appears and the total absorbance is considerably increased. This change increases when adding more TBP, see Fig. S13a.† The TBP-induced spectral changes implies that TBP present in the solution must influence the inner coordination sphere of the Co(III) complex and in some way lower the symmetry of the coordination. ^{1}H-NMR spectroscopy can be used to monitor the TBP. A slight downfield shift was found for the TBP 2*H*-pyridine (peak a, at ~7.35 ppm) upon mixing and by comparing ^{1}H NMR spectra of TBP alone to that of a mixture with $[Co(bpy)_3]^{3+}$, see Fig. 7. Furthermore, peak a shifts back (hidden in the 2*H*-bpy peak at ~7.40 ppm) when extra ligand, bipyridine (bpy), is added to the solution, while the characteristic peaks and the d–d absorption spectra of $[Co(bpy)_3]^{3+}$ remain unchanged, see Fig. S14.† It is here notable that the NMR spectra show a significant difference in the dynamics of ligand exchange between bpy and TBP, where TBP clearly is involved in a fast exchange with Co(III) and bpy is characterized by a slow exchange. Nevertheless, the NMR spectra show that some sort of ligand exchange affecting the chemical environment of TBP must take place. The effects of adding TBP to a solution/electrolyte containing $[Co(bpy)_3]^{3+}$ must involve a change in the coordination geometry of $[Co(bpy)_3]^{3+}$.[48] There are however no clues in the spectroscopic results to what type of coordination that may take place. Considering the fast TBP exchange, a general expression of ligand effect can be formulated (eqn (2)). Such an in-binding of TBP may or may not cause a dissociation of bpy, and thus x and y are unknown in eqn (2). Considering that the TBP exchange is fast and the bpy exchange is slow, it seems unlikely that a Co(III) complex of lower coordination number than 6 is formed. Quantum-chemical calculations on initial 7-coordinate $[Co(bpy)_3(TBP)]^{3+}$ complexes converge to quasi-octahedral, 6-coordinate species, where bpy ligands placed *trans* to TBP are shifted sideways to release the

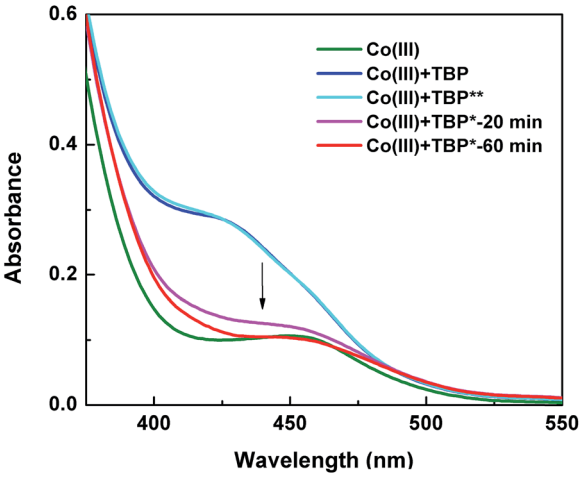

Fig. 6 UV-vis absorption spectra of $[Co(bpy)_3]^{3+}$ only (green), $[Co(bpy)_3]^{3+}$/TBP in acetonitrile before (blue) and after storage in the dark (light blue) and after light illumination for 20 min (pink) and 60 min (red).

coordination of one of its two pyridine N-atoms. Thus, also higher coordination numbers than 6 appear less feasible. Nevertheless, a lowering of the Co(III) coordination symmetry, possibly *via* effects from TBP in the second coordination shell of Co(III), as proposed by Salim and co-workers,[21] could cause a splitting of the molecular orbitals dominated by the Co d-orbitals. Such a splitting may both change the magnetic properties of the complex and certainly affect the strength of the d–d-transitions, which is thus consistent with the new UV-vis spectral feature observed.

$$[Co(bpy)_3]^{3+} + x\text{TBP} \rightleftharpoons [Co(bpy)_y(TBP)_x]^{3+} + (3-y)\text{bpy} \quad (2)$$

Using the NMR-spectroscopic data focusing on the exchange of TBP, the exchange equilibrium constant can be estimated ($K = 3.7 \times 10^{-3}$, see Table S8†). In such an estimate changes in bpy coordination are neglected. Consequently, we can deduce that only one to a few percent of the $[Co(bpy)_3]^{3+}$ will be converted according to eqn (2) in the normal DSSC electrolyte, making it hard to identify the exact structure of the resulting Co(III) complex of lower symmetry. Such effects are drowned by the predominantly present and symmetrical $[Co(bpy)_3]^{3+}$ ions. From the results in Table 2, the most dramatic change in diffusive properties is observed for TBP, decreasing from about 24×10^{-10} m^2 s^{-1} to 15×10^{-10} m^2 s^{-1} when mixed with the $[Co(bpy)_3]^{3+}$ ions in acetonitrile. This indicates that in a dilute solution for ^{1}H-NMR spectroscopic investigations, at least 40% of the added TBP in some way interacts with the $[Co(bpy)_3]^{3+}$ complexes and slightly reduces the mobility of the Co(III) ions (9.6×10^{-10} m^2 s^{-1} to 8.7×10^{-10} m^2 s^{-1}) in the bulk solution. In summary, the spectroscopic results demonstrate an interaction between $[Co(bpy)_3]^{3+}$ and TBP, which irrespective if involving a ligand exchange or only a secondary interaction, could be the nature of the favourably shielding effect of TBP on electron recombination to Co(III) acceptors as reported and the adverse retarding effect on the electrolyte diffusion as discussed above.

After the $[Co(bpy)_3]^{3+}$/TBP mixture has been exposed to light, the d–d absorption intensity decreases with time and end up close to the spectrum of the pure and untreated solution of $[Co(bpy)_3]^{3+}$. ^{1}H NMR spectra show that the TBP peak (a) is broadened (Fig. S15†) and changed back to a sharp peak when extra bpy is added from the start (Fig. 7) or added afterwards (Fig. S16†). In Fig. 7, it can be clearly observed that the peak a further and gradually shifts downfield with light exposure time, as also observed for the water peak (~2.25 ppm). A concomitant new peak (henceforth identified as Co′) arises at ~14.5 ppm. These phenomena are not observed for the same mixture stored in dark (Fig. 6 and S17†). The spectral changes are irreversible after turning off the light. Since TBP exchange is fast, the original state of the $[Co(bpy)_3]^{3+}$/TBP system will not be re-formed (otherwise it would again partially go back to the asymmetric species with strong d–d absorption, as described above, immediately after turning off the light). The decrease in the Co(III) d–d absorption intensity as function of light exposure time was studied by varying the initial concentrations of $[Co(bpy)_3]^{3+}$ and TBP, see Fig. S13b,† highlighting that the change rate is related to the concentrations of the two compounds. Thus, an irreversible chemical reaction is indicated to take place between the two components upon light exposure. The spectral change is much more difficult to model, but combined with the ^{1}H-NMR-spectroscopic results shown in Fig. 7, it is clear that $[Co(bpy)_3]^{3+}$ is still the main species present in solution, and it must return to a pseudo-octahedral configuration (weak d–d transitions) after light exposure. The Raman spectra in Fig. S18a† show that a new peak arises with a 27 cm^{-1} shift with respect to the TBP ring breathing frequency at ~997 cm^{-1}. IR-spectroscopic results shown in Fig. S18b† display a similar qualitative effect, where the pyridine ring vibration modes (δ(C–H), 765 cm^{-1} and 819 cm^{-1}) decrease in

Table 2 Diffusion coefficients (D) of compounds in the electrolytes and effective charges (Z_{eff}) of $Co(bpy)_3^{3+}$ extracted from *in situ* diffusion ^{1}H-NMR spectroscopic measurements

Samples	D_{TBP}[a] ($\times 10^{-10}$ m^2 s^{-1})	D_{CoB_3} ($\times 10^{-10}$ m^2 s^{-1})	$D_{Co'}$ ($\times 10^{-10}$ m^2 s^{-1})	Z_{eff}
$[Co(bpy)_3^{3+}]$	—	9.6	—	1.38
TBP	23.9	—	—	0
$[Co(bpy)_3^{3+}]$/TBP-fresh	15.4	8.7	—	1.34
$[Co(bpy)_3^{3+}]$/TBP-light	18.2	8.5	9.0	1.20

[a] Derived from the peak a.

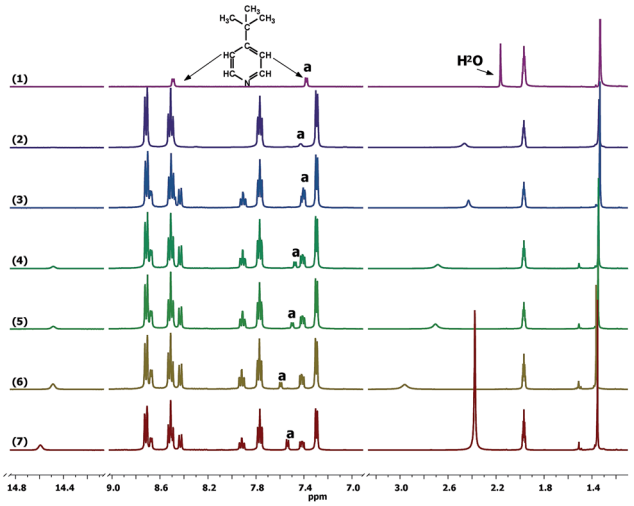

Fig. 7 ^{1}H NMR spectra of (1) TBP only, (2) $[Co(bpy)_3]^{3+}$/TBP, (3) $[Co(bpy)_3]^{3+}$/TBP/bpy when fresh and after light exposure for (4) 2 h, (5) 4 h and (6) 24 h, and (7) with one more equivalent of fresh TBP added in CD_3CN. The characteristic peak of the TBP pyridine hydrogen atoms is labelled a. The initial component concentrations were: TBP 0.008 M, $[Co(bpy)_3]^{3+}$ 0.05 M and bpy 0.05 M.

intensity after light exposure. The Raman downshift in wavenumbers, which indicates a lower ring binding strength or alternatively a higher effective mass affecting the ring vibration, could be attributed to TBP either becoming coordinated to the cobalt centre or protonated.[49–51] However, a persistent coordination to Co(III) is not a feasible explanation because of the observed fast TBP ligand exchange. The shift of the TBP peak a is reduced either when adding fresh TBP to the exposed mixture (the integral intensity increases as well, Fig. 7) or when more TBP is added from the start, see Fig. S19.† This demonstrates that the peak corresponds to the weighted average of a free/modified TBP system in the fast exchange regime with respect to the frequency difference between the spin systems (peaks) involved. In this context we also note that the diffusion coefficient of TBP after light exposure is still lower than that of free TBP.

It is also worth noting that the Co′ ^{1}H NMR-spectroscopic peak with a chemical shift at around 14.5 ppm, alluded to above, emerges and increases with time of light exposure. The peak areas indicate that part of Co(III) has been converted into this new species. The peak shows a short relaxation time (T_1 = 0.082 s) and stronger temperature dependence (Fig. S20†), indicating the formation of a paramagnetic complex. Possible explanations to this new peak include (1) the formation of paramagnetic Co(II) (d^7 configuration) involving a redox reaction;[52] (2) a light-induced spin-crossover of Co(III) to a high-spin state driven by TBP.[53,54] A third alternative could involve the generation of a binuclear complex coordinated by TBP, but the essentially unaffected diffusion coefficients of the Co-containing species speak against such an explanation.[55,56] These hypothesized complexes cannot be detected by QC-MS, see Fig. S21.† In fact, all attempts to isolate any new species from the $[Co(bpy)_3]^{3+}$–TBP mixtures, light-exposed or not, have resulted in solid compounds containing the pure $[Co(bpy)_3]^{3+}$ complex only. We have observed that in the presence of $[Co(bpy)_3]^{3+}$, addition of the $[Co(bpy)_3]^{2+}$ complex to a TBP solution leads to a broadened TBP peak a in ^{1}H-NMR spectra (Fig. S22†), which is consistent with that in the presence of $[Co(bpy)_3]^{3+}$ after light exposure. The reason could be fast ligand exchange between TBP and the labile paramagnetic Co(II) species. Thus, the fact that extra addition of bpy to the light-exposed system leads to sharper TBP peaks is understandable, as a TBP/bpy ligand exchange equilibrium at the Co(II) centre is reformed. Hence, scenario (1) is more reasonable; that is, a redox reaction occurs in the $[Co(bpy)_3]^{3+}$/TBP system under light with $[Co(bpy)_3]^{2+}$ being formed. Redox reaction products of TBP or bpy are unlikely to explain the spectral changes, but more likely reaction with some unintentional electrolyte component, such as water.[57] A possible reaction is proposed in eqn (3).

$$4[Co(bpy)_3]^{3+} + 2H_2O + TBP \rightarrow 4[Co(bpy)_3]^{2+} + 4TBP\text{–}H^+ + O_2 \quad (3)$$

The production of protons binding to the base TBP could be inferred by the gradual downfield shift of the TBP peak a and water peak in Fig. 7.[50,51] The hard acidity of protons is similar to that of Li^+ ions, and so are the effects on DSSCs, including those on the photoanode, such as the positively shifted E_c, the red-shifted absorption spectra of the dye/TiO_2 film, the suppressed recombination loss and for the other part, reduced TBP activity in interacting with $[Co(bpy)_3]^{3+}$ due to protonation, allowing $[Co(bpy)_3]^{3+}$ to go back to a symmetric configuration with weak d–d light absorption. Since no significant increase is observed for the diffusion coefficients of Co(III) and Co′ after light exposure, the enhancement of diffusion/charge transport is likely to be attributed to the reduction of available TBP at the cathode surface due to protonation. Thus, by the strategy of light exposure on $[Co(bpy)_3]^{3+}$/TBP mixture with a possible production of protons as a result, the DSSC performance reaches the same levels as when Li^+ salts have been added. In addition, the presence of Li^+ salts shows worse dye photostability than the presence of a Brønsted acid (Fig. S23†). This result explains the benefits of the Li^+-ion-free cobalt electrolytes with respect to the long-term photostability of DSSCs.

Conclusions

This work has identified an irreversible light-induced reaction in the commonly used cobalt tris-(bipyridine)-mediated electrolyte for DSSCs. This effect causes a significant improvement of cell performance, mainly in the photocurrent. After prior light exposure treatment of a Co(III)/TBP mixture, solar cells outperform typical lithium-ion-containing ones both regarding initial conversion efficiency and long-term stability. Detailed characterization based on fully operational devices, as well as model systems containing electrolyte mixtures, points to an interaction between Co(III) and TBP, which macroscopically influences the kinetics at the electrode/electrolyte interfaces. The microscopic picture remains a bit unclear, although we can

present a plausible explanation to a $[Co(bpy)_3]^{3+}$–TBP interaction upon mixing, based on secondary coordination, and to a proposed redox reaction between Co(III) with trace water in the presence of TBP upon light exposure leading to the formation of protons or TBP protonation. All in all, the work points to the importance of investigating the detailed molecular dynamics in multi-component DSSC systems, and particularly regarding the electrolyte and its interface reactions.

Conflicts of interest

There are no conflicts of interest to declare.

Acknowledgements

We gratefully acknowledge the Swedish Research Council, the Swedish Energy Agency as well as the China Scholarship Council (CSC) for financial support. The authors also thank Dr Lei Wang for his helpful assistance in ^{1}H-NMR spectroscopic studies.

Notes and references

1 B. O'Regan and M. Grätzel, *Nature*, 1991, **353**, 737–740.
2 J. Gao, M. Bhagavathi Achari and L. Kloo, *Chem. Commun.*, 2014, **50**, 6249–6251.
3 J. Gao, W. Yang, M. Pazoki, G. Boschloo and L. Kloo, *J. Phys. Chem. C*, 2015, **119**, 24704–24713.
4 T. C. Li, A. M. Spokoyny, C. She, O. K. Farha, C. A. Mirkin, T. J. Marks and J. T. Hupp, *J. Am. Chem. Soc.*, 2010, **132**, 4580–4582.
5 B. A. Gregg, F. Pichot, S. Ferrere and C. L. Fields, *J. Phys. Chem. B*, 2001, **105**, 1422–1429.
6 T. W. Hamann, *Dalton Trans.*, 2012, **41**, 3111–3115.
7 S. M. Feldt, E. A. Gibson, E. Gabrielsson, L. Sun, G. Boschloo and A. Hagfeldt, *J. Am. Chem. Soc.*, 2010, **132**, 16714–16724.
8 S. M. Feldt, P. W. Lohse, F. Kessler, M. K. Nazeeruddin, M. Gratzel, G. Boschloo and A. Hagfeldt, *Phys. Chem. Chem. Phys.*, 2013, **15**, 7087–7097.
9 Y. Xie, J. Baillargeon and T. W. Hamann, *J. Phys. Chem. C*, 2015, **119**, 28155–28166.
10 M. K. Kashif, J. C. Axelson, N. W. Duffy, C. M. Forsyth, C. J. Chang, J. R. Long, L. Spiccia and U. Bach, *J. Am. Chem. Soc.*, 2012, **134**, 16646–16653.
11 M. K. Kashif, M. Nippe, N. W. Duffy, C. M. Forsyth, C. J. Chang, J. R. Long, L. Spiccia and U. Bach, *Angew. Chem., Int. Ed.*, 2013, **52**, 5527–5531.
12 Y. Xie and T. W. Hamann, *J. Phys. Chem. Lett.*, 2013, **4**, 328–332.
13 B. M. Klahr and T. W. Hamann, *J. Phys. Chem. C*, 2009, **113**, 14040–14045.
14 H. Nusbaumer, S. M. Zakeeruddin, J.-E. Moser and M. Grätzel, *Chem.–Eur. J.*, 2003, **9**, 3756–3763.
15 S. M. Feldt, U. B. Cappel, E. M. J. Johansson, G. Boschloo and A. Hagfeldt, *J. Phys. Chem. C*, 2010, **114**, 10551–10558.
16 J.-H. Yum, E. Baranoff, F. Kessler, T. Moehl, S. Ahmad, T. Bessho, A. Marchioro, E. Ghadiri, J.-E. Moser, C. Yi, M. K. Nazeeruddin and M. Grätzel, *Nat. Commun.*, 2012, **3**, 631.
17 E. Mosconi, J.-H. Yum, F. Kessler, C. J. Gómez García, C. Zuccaccia, A. Cinti, M. K. Nazeeruddin, M. Grätzel and F. De Angelis, *J. Am. Chem. Soc.*, 2012, **134**, 19438–19453.
18 S. Nakade, Y. Makimoto, W. Kubo, T. Kitamura, Y. Wada and S. Yanagida, *J. Phys. Chem. B*, 2005, **109**, 3488–3493.
19 J. J. Nelson, T. J. Amick and C. M. Elliott, *J. Phys. Chem. C*, 2008, **112**, 18255–18263.
20 T. N. Murakami, N. Koumura, T. Uchiyama, Y. Uemura, K. Obuchi, N. Masaki, M. Kimura and S. Mori, *J. Mater. Chem. A*, 2013, **1**, 792–798.
21 N. T. Salim, X. Yang, S. Zhang, J. Liu, A. Islam and L. Han, *J. Mater. Chem. A*, 2014, **2**, 10532–10539.
22 W. Yang, Y. Hao, P. Ghamgosar and G. Boschloo, *Electrochim. Acta*, 2016, **213**, 879–886.
23 J. T. Kirner and C. M. Elliott, *J. Phys. Chem. C*, 2015, **119**, 17502–17514.
24 A. Listorti, C. Creager, P. Sommeling, J. Kroon, E. Palomares, A. Fornelli, B. Breen, P. R. F. Barnes, J. R. Durrant, C. Law and B. O'Regan, *Energy Environ. Sci.*, 2011, **4**, 3494–3501.
25 L. Yang, B. Xu, D. Bi, H. Tian, G. Boschloo, L. Sun, A. Hagfeldt and E. M. J. Johansson, *J. Am. Chem. Soc.*, 2013, **135**, 7378–7385.
26 P. Tiwana, P. Docampo, M. B. Johnston, L. M. Herz and H. J. Snaith, *Energy Environ. Sci.*, 2012, **5**, 9566–9573.
27 B. O'Regan and D. T. Schwartz, *Chem. Mater.*, 1998, **10**, 1501–1509.
28 S. Ferrere and B. A. Gregg, *J. Phys. Chem. B*, 2001, **105**, 7602–7605.
29 B. A. Gregg, S.-G. Chen and S. Ferrere, *J. Phys. Chem. B*, 2003, **107**, 3019–3029.
30 M. Bhagavathi Achari, V. Elumalai, N. Vlachopoulos, M. Safdari, J. Gao, J. M. Gardner and L. Kloo, *Phys. Chem. Chem. Phys.*, 2013, **15**, 17419–17425.
31 J. Nissfolk, K. Fredin, A. Hagfeldt and G. Boschloo, *J. Phys. Chem. B*, 2006, **110**, 17715–17718.
32 M. Bailes, P. J. Cameron, K. Lobato and L. M. Peter, *J. Phys. Chem. B*, 2005, **109**, 15429–15435.
33 K. C. D. Robson, K. Hu, G. J. Meyer and C. P. Berlinguette, *J. Am. Chem. Soc.*, 2013, **135**, 1961–1971.
34 L. J. Antila, F. G. Santomauro, L. Hammarström, D. L. Fernandes and J. Sá, *Chem. Commun.*, 2015, **51**, 10914–10916.
35 S. Sarker, A. J. S. Ahammad, H. W. Seo and D. M. Kim, *Int. J. Photoenergy*, 2014, **2014**, 17.
36 F. Hallberg, I. Furó, P. V. Yushmanov and P. Stilbs, *J. Magn. Reson.*, 2008, **192**, 69–77.
37 G. W. T. M. J. Frisch, H. B. Schlegel, G. E. Scuseria, M. A. Robb, J. R. Cheeseman, G. Scalmani, V. Barone, B. Mennucci, G. A. Petersson, H. Nakatsuji, M. Caricato, X. Li, H. P. Hratchian, A. F. Izmaylov, J. Bloino, G. Zheng, J. L. Sonnenberg, M. Hada, M. Ehara, K. Toyota, R. Fukuda, J. Hasegawa, M. Ishida, T. Nakajima, Y. Honda, O. Kitao, H. Nakai, T. Vreven, J. A. Montgomery Jr, J. E. Peralta, F. Ogliaro, M. Bearpark, J. J. Heyd, E. Brothers, K. N. Kudin, V. N. Staroverov, R. Kobayashi,

J. Normand, K. Raghavachari, A. Rendell, J. C. Burant, S. S. Iyengar, J. Tomasi, M. Cossi, N. Rega, J. M. Millam, M. Klene, J. E. Knox, J. B. Cross, V. Bakken, C. Adamo, J. Jaramillo, R. Gomperts, R. E. Stratmann, O. Yazyev, A. J. Austin, R. Cammi, C. Pomelli, J. W. Ochterski, R. L. Martin, K. Morokuma, V. G. Zakrzewski, G. A. Voth, P. Salvador, J. J. Dannenberg, S. Dapprich, A. D. Daniels, Ö. Farkas, J. B. Foresman, J. V. Ortiz, J. Cioslowski and D. J. Fox, *Gaussian 09, Revision E.01*, Gaussian, Inc., Wallingford CT, 2009.

38 T. Yanai, D. P. Tew and N. C. Handy, *Chem. Phys. Lett.*, 2004, **393**, 51–57.

39 M. Dolg, U. Wedig, H. Stoll and H. Preuss, *J. Chem. Phys.*, 1987, **86**, 866–872.

40 J. M. L. Martin and A. Sundermann, *J. Chem. Phys.*, 2001, **114**, 3408–3420.

41 S. Agrawal, T. Leijtens, E. Ronca, M. Pastore, H. Snaith and F. De Angelis, *J. Mater. Chem. A*, 2013, **1**, 14675–14685.

42 W. Yang, Y. Hao, N. Vlachopoulos, A. I. K. Eriksson and G. Boschloo, *J. Phys. Chem. C*, 2016, **120**, 22215–22224.

43 R. M. O'Donnell, R. N. Sampaio, T. J. Barr and G. J. Meyer, *J. Phys. Chem. C*, 2014, **18**, 16976–16986.

44 J. Wiberg, T. Marinado, D. P. Hagberg, L. Sun, A. Hagfeldt and B. Albinsson, *J. Phys. Chem. B*, 2010, **114**, 14358–14363.

45 R. Gao, L. Wang, Y. Geng, B. Ma, Y. Zhu, H. Dong and Y. Qiu, *Phys. Chem. Chem. Phys.*, 2011, **13**, 10635–10640.

46 J. Teuscher, J.-D. Décoppet, A. Punzi, S. M. Zakeeruddin, J.-E. Moser and M. Grätzel, *J. Phys. Chem. Lett.*, 2012, **3**, 3786–3790.

47 T. M. Koh, K. Nonomura, N. Mathews, A. Hagfeldt, M. Grätzel, S. G. Mhaisalkar and A. C. Grimsdale, *J. Phys. Chem. C*, 2013, **117**, 15515–15522.

48 J. T. Kirner and C. M. Elliot, *J. Phys. Chem. C*, 2015, **119**, 17502–17514.

49 L. Kavan, Y. Saygili, M. Freitag, S. M. Zakeeruddin, A. Hagfeldt and M. Grätzel, *Electrochim. Acta*, 2017, **227**, 194–202.

50 G. Roy, J. F. Miravet, B. Escuder, C. Sanchez and M. Llusar, *J. Mater. Chem.*, 2006, **16**, 1817–1824.

51 N. Wattanavichean, E. Casey, R. J. Nicholsa and H. Arnolds, *Phys. Chem. Chem. Phys.*, 2018, **20**, 866–871.

52 J. K. Beattie and H. Elsbernd, *Inorg. Chim. Acta*, 1995, **240**, 641–644.

53 M. Khalil, M. A. Marcus, A. L. Smeigh, J. K. McCusker, H. H. W. Chong and R. W. Schoenlein, *J. Phys. Chem. A*, 2006, **110**, 38–44.

54 S. Thies, H. Sell, C. Schütt, C. Bornholdt, C. Näther, F. Tuczek and R. Herges, *J. Am. Chem. Soc.*, 2011, **133**, 16243–16250.

55 Ş. Yurdakul and M. Banat, *J. Inclusion Phenom. Macrocyclic Chem.*, 1996, **26**, 127–131.

56 M. Fondo, N. Ocampo, A. M. Garcia-Deibe, M. Corbella, M. S. El Fallah, J. Cano, J. Sanmartin and M. R. Bermejo, *Dalton Trans.*, 2006, 4905–4913, DOI: 10.1039/b609961k.

57 J. Gao, A. Fischer, P. H. Svensson and L. Kloo, *ChemistrySelect*, 2017, **2**, 1675–1680.